

Check for updates

1D ZrCl₄ Matrices for Enhanced Ion Transport in Glassy **Chloride Electrolytes**

Yongli Song, Shida Xue, Zijin Xu, Jianjun Fang, Zhaohuang Zhan, Yao-Hui Wang, Chuanxi Chen, Shunning Li, Tongchao Liu, Yong Yang, Luyi Yang,* and Feng Pan*

Designing a solid-state electrolyte (SSE) that combines the lithium-ion transport behavior found in liquid or solid polymer electrolytes with the high lithium-ion transference number characteristic of inorganic SSEs is an immensely appealing challenge. Herein, a cost-effective, chain-structured ZrCl₄ is introduced as a hosting matrix, resembling polyethylene oxide (PEO), to facilitate the dissociation of lithium salts (e.g., LiCl, Li₂SO₄, and Li₃PO₄). The dissociated free Li-ions can be coordinated by the [ZrCl₆] octahedra, forming fast ion-conducting pathways along ZrCl₄ chains that achieve an ionic conductivity as high as 1.2 mS cm⁻¹. Simultaneously, ZrCl₄ serves as a Lewis acid, trapping anions and delivering a high lithium transference number approaching unit. The proposed electrolyte exhibits stable cycling performance when integrated into LiNi_{0.8}Mn_{0.1}Co_{0.1}O₂||Li-In cells. Moreover, this design strategy also extends to the synthesis of sodium-ion conductors, achieving a high ionic conductivity of 0.3 mS cm⁻¹. Demonstrating a previously unreported lithium-ion conduction mechanism, the proposed ZrCl₄-based electrolytes offer a versatile approach for tailoring advanced SSEs.

Y. Song, S. Xue, Z. Xu, J. Fang, Z. Zhan, C. Chen, S. Li, L. Yang, F. Pan School of Advanced Materials

Peking University

Shenzhen Graduate School Shenzhen 518055, China

E-mail: yangly@pkusz.edu.cn; panfeng@pkusz.edu.cn

Y. Song

School of Energy and Power Engineering

Jiangsu University

Zhenjiang 212013, China

Y.-H. Wang

College of Materials

Xiamen University

Xiamen 361005, China

Chemical Sciences and Engineering Division

Argonne National Laboratory

Argonne, IL 60439, USA

College of Chemistry and Chemical Engineering Xiamen University

Xiamen 361005, China



The ORCID identification number(s) for the author(s) of this article

DOI: 10.1002/aenm.202500913

1. Introduction

Solid-state batteries (SSBs) are considered an ideal next-generation electrochemical energy storage system to replace commercial lithium-ion batteries due to their potentially higher intrinsic safety and energy densities.[1,2] One key aspect of developing SSBs is to design SSEs with both high ionic conductivity and a wide electrochemical window.[3,4] The capability of Li+ conduction in SSEs is largely determined by the chemical environment of Li+ and the corresponding Li+ transport pathways.^[5-7] Ideally, Li⁺ should be able to move anisotropically as they do in liquid electrolytes[8] One resembling example is the Li⁺ transfer mechanism in polymeric SSEs such as PEO, where Li+ is solvated by polymer segments via the strong Li-O coordination. [9-11] However, due to the strong coordination between Li+ and polymer chains,

the conduction of Li⁺ is also limited by the sluggish polymer motion under room temperature and the low Li+ transference number (generally lower than 0.5).[12-14] Therefore, exploring a solid electrolyte that enables free and efficient Li⁺ transport is of great significance.

Glass-type solid electrolytes, characterized by isotropic nature and low grain boundary resistance, hold great promise for meeting the above requirements. The glassy state design has been widely adopted in SSEs such as sulfides, metalorganic frameworks, and chlorides.[15-19] Compared with sulfides, chloride-based electrolytes demonstrated significant advantages in environmental friendliness and high oxidative stability (>4.3 V vs Li+/Li), which are suitable for high-voltage cathodes.[20-22] Although chlorides are generally unstable to lithium-metal anodes, a sulfide buffer layer (e.g., Li₆PS₅Cl) can effectively prevent their degradation without unduly increasing interfacial impedance.[23-25] More recently, Hu and coworkers developed an oxygen-substituted chloride electrolyte $MAlCl_{4.2x}O_x$ (M = Li, Na) with high ionic conductivity, confirming the potential of glassy chloride applications. [26] However, the lack of long-range periodicity in glassy SSEs hinders the understanding and modulation of ion transport. Therefore, exploring the intrinsic structural features of chlorides and their impact on ion transport is essential for

16146840, 2025, 30, Downloaded from https://advancec

.com/doi/10.1002/aenm.202500913 by University Town Of Shenzhen, Wiley Online Library on [17/11/2025]. See the Terms

on Wiley Online Library for rules of use; OA articles are governed by the applicable Creative Commons

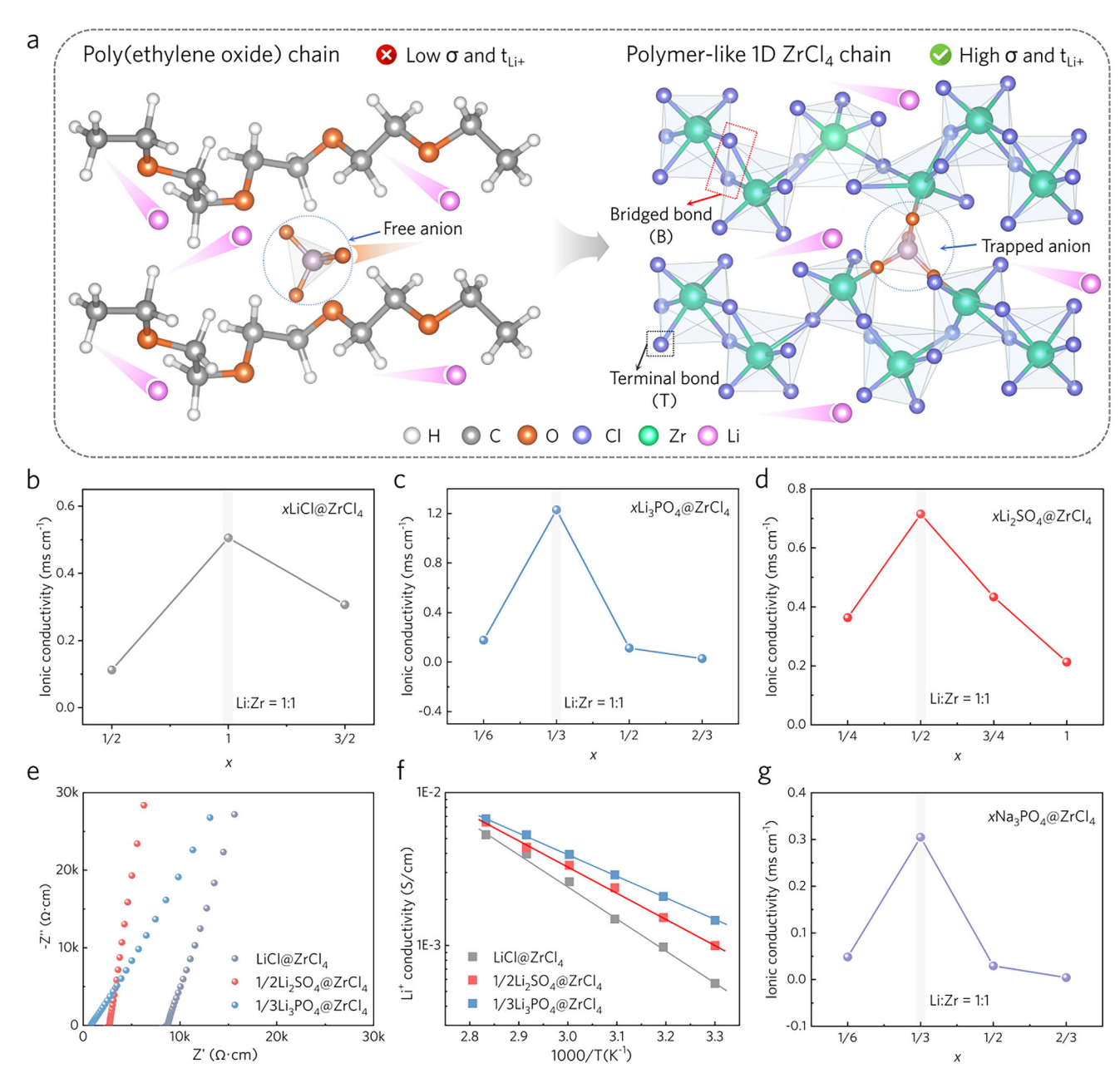


Figure 1. Design schematic and Li-ion conducting properties of SSEs. a) Schematic of anions trapped by polymer-like ZrCl₄ matrix to release free Li ions for fast conduction. b–d) Ionic conductivity is dependent on lithium salt concentration for different SSEs. e) Nyquist plots of the EIS measurement results of SSEs. f) Arrhenius plots of the SSEs. g) Ionic conductivity depends on the Na₃PO₄ concentration of xNa₃PO₄@ZrCl₄.

developing glassy chlorides with ideal ion transport mechanisms.

As a low-cost quasi 1D compound, $ZrCl_4$ exhibits characteristic signatures of zigzag, PEO-like chain-structured $[(ZrCl_{4/2})Cl_2]_n$ with Cl-bridged edge-sharing $[ZrCl_6]$ octahedra, where Cl atoms at bridge positions and terminal positions are marked as Cl(B) and Cl(T), respectively. These parallelly arranged chains are held together by van der Waals forces rather than chemical bonds (Figure S1, Supporting Information), potentially facilitating abundant pathways for Li⁺ conduction. Besides, as described in Figure 1a, $ZrCl_4$ is a natural Lewis acid, which tends to trap

anions, thus dissociating ion pairs in Li salts. Therefore, "dissolving" Li salts in ${\rm ZrCl_4}$ might be an effective way to obtain solid electrolytes with high ionic conductivity.

In this work, a class of solid electrolytes based on ZrCl₄ with high ionic conductivity (1.2 mS cm⁻¹) was prepared using the facile ball milling method. By thoroughly mixing lithium salts with ZrCl₄, Li⁺ can be coordinated by the ZrCl₄ octahedra without interrupting the chain structure, thus ensuring the integrity of the Li⁺ transport channels. Compared with liquid/polymer electrolytes, the as-prepared solid electrolyte has an ion migration number close to the integer because the anions are also bound by

www.advancedsciencenews.com

www.advenergymat.de

ADVANCED ENERGY MATERIALS 16146484, 2025, 30, Dwnholaded from https://dwnneed.onlinelibrary.wiely.com/d/010.002/aen.20.2020913 by University Town Of Sheraben, Wiley Online Library on [17/11/1025]. See he Terms and Conditions (https://onlinelibrary.wiely.com/terms-and-conditions) on Wiley Online Library for rules of use; OA articles are governed by the applicable Cerative Commons

the $[ZrCl_6]$ octahedra chain. The design strategy presented here can also be applied to the design of fast sodium-ion conductors, demonstrating good versatility.

ence number ($t_{\rm Li+}$) was calculated to be 0.90, indicating that lithium ions are the primary conducting carriers.^[33]

2. Results and Discussion

2.1. Li-Ion Conducting Properties

SSEs based on ZrCl4 were prepared by ball-milling a stoichiometric mixture of lithium salt and ZrCl4. In this case, three low-cost lithium salts with monovalent (LiCl), divalent (Li₂SO₄), and trivalent (Li₃PO₄) anions were selected. Room-temperature impedance spectra (Figure S2, Supporting Information) and ionic conductivity of SSEs with various Li: Zr ratios (Figure 1b-d) show that all three lithium salts can be ball milled with ZrCl₄ to form SSEs with high ionic conductivity ($>10^{-4}$ S cm⁻¹). In terms of room-temperature conductivity, the optimized ratios are LiCl@ZrCl₄ (0.5 mS cm⁻¹), 1/2Li₂SO₄@ZrCl₄ (0.7 mS cm⁻¹), and 1/3Li₃PO₄@ZrCl₄ (1.2 mS cm⁻¹), respectively. It is worth noting that for all Li salts, the highest ionic conductivity can be obtained when $[Li^+]$: $[ZrCl_4] = 1$, suggesting Li^+ transport behaviors follow the same mechanism in this type of SSE. In addition, the room-temperature Nyquist plots (Figure 1e) show that without high-temperature sintering, the solid electrolyte containing three anions exhibits negligible grain boundary resistance, manifesting characteristics of glass-type solid electrolytes. Moreover, based on the temperature-dependent impedance spectra (Figure \$3, Supporting Information), the activation energies of LiCl@ZrCl₄, 1/2Li₂SO₄@ZrCl₄, and 1/3Li₃PO₄@ZrCl₄ samples are calculated to be 0.42, 0.31, and 0.28 eV, respectively (Figure 1f). Since Li₃PO₄-based electrolytes outperformed other electrolytes in terms of conductivity, we will focus on analyzing this type of solid electrolyte.

In principle, the chain-like structure of ZrCl₄, resembling that of PEO, should be capable of facilitating the fast conduction of other alkali metal ions. Here, xNa₃PO₄@ZrCl₄ compounds were synthesized and tested. Similar to xLi₃PO₄@ZrCl₄, the ionic conductivity at room temperature of xNa₃PO₄@ZrCl₄ (Figure 1g) shows a maximum of 0.33 mS cm⁻¹ when the ratio of Na: Zr is 1:1, and the calculated activation energy (Figure S4, Supporting Information) of 1/3Na₃PO₄@ZrCl₄ (0.27 eV) is almost identical to that of 1/3Li₃PO₄@ZrCl₄. Therefore, it is reasonable to speculate that Na⁺ shares the same transport mechanism as Li⁺, attributed to the low structural rigidity and ion-size selectivity caused by weak van der Waals forces between ZrCl₄ chains. However, the larger ionic radius of Na⁺ slows its transport, resulting in lower ionic conductivity than Li⁺ conductors.

An ideal SSE for Li-ion batteries should solely transport Li⁺. However, the high electronic conductivity of some ceramic SSEs and anionic mobility in PEO-based polymeric SSEs have raised a series of issues. [30,31] Via the blocking electrode polarization method, the electronic conductivity of $1/3 \text{Li}_3 \text{PO}_4 @ \text{ZrCl}_4$ is measured to be $3.9 \times 10^{-9} \text{ S cm}^{-1}$ (Figure S5, Supporting Information), which is about six orders of magnitude lower than its ionic conductivity, showing excellent safety for high-power application scenarios. [32] According to direct current measurement of $1/3 \text{Li}_3 \text{PO}_4 @ \text{ZrCl}_4$ sandwiched by $\text{Li}_2 \text{S-P}_2 \text{S}_5$ SSEs and Li-metal (Figure S6, Supporting Information), the lithium-ion transfer-

2.2. Characterization of xLi₃PO₄@ZrCl₄

The X-ray Diffraction (XRD) patterns of various $\alpha \text{Li}_3 \text{PO}_4 \otimes \text{ZrCl}_4$ composites (Figure 2a) show that with a relatively smaller amount of Li_3PO_4 (x = 1/6 or 1/3), the obtained SSEs exist in amorphous form. The broad diffraction band ≈18° should be attributed to the polyimide film covering the samples, which was applied to protect the chlorides from moisture due to their sensitivity to air humidity (Figure S7, Supporting Information). The 1/3Li₃PO₄@ZrCl₄ was pressed into a tablet and thinned using a focused ion beam (FIB) for high-resolution transmission electron microscopy (HRTEM) analysis. The amorphous nature of 1/3Li₃PO₄@ZrCl₄ is further confirmed by HRTEM images of both the bulk and edge regions, as well as the corresponding overall fast Fourier transform (FFT) patterns (Figure S8, Supporting Information), where no distinct lattice fringes or diffraction spots are observed. Additionally, elemental mapping images reveal a uniform distribution of elements without any detectable phase separation (Figure S9, Supporting Information). Differential scanning calorimetry analysis indicates the glassy state of $1/3 \text{Li}_3 \text{PO}_4 \otimes \text{ZrCl}_4$, with a glass transition temperature (T_a) of ≈225 °C (Figure S10, Supporting Information). Scanning electron microscopy (SEM) images show indistinct grain boundaries and irregular grain structures, presenting a dense morphology characteristic of a molten-like or glassy state (Figure S11, Supporting Information). With the increase of Li₃PO₄ content in the samples, the diffraction peak of LiCl begins to manifest instead of Li₃PO₄. Therefore, it could be speculated that Li₃PO₄ is gradually dissociated by ZrCl₄, with PO₄³⁻ ions being anchored by the polymer-like chains of ZrCl₄. Nevertheless, the excess Li₃PO₄ disrupts the Zr-Cl chains by breaking the Zr-Cl bonds, leading to the precipitation of LiCl. The existence of crystalline LiCl can also be observed from the TEM image (Figure \$12, Supporting Information). The variation tendency in XRD patterns of xLiCl@ZrCl₄ and xLi₂SO₄@ZrCl₄ (Figure S13, Supporting Information) is very similar to that of xLi₃PO₄@ZrCl₄, suggesting similar evolution processes for the chemical environment of Li⁺ in ZrCl₄-based SSEs.

Next, the atomic pair distribution function (PDF) technique is employed to investigate the local structure changes in xLi₃PO₄@ZrCl₄ SSEs and the salt dissociation mechanism. All peaks in the PDF pattern of ZrCl₄ (Figure \$14, Supporting Information) can be assigned accordingly based on Figure S15 (Supporting Information), with peaks at ≈ 2.19 , ≈ 2.55 , ≈ 3.15 , and \approx 3.56 Å sequentially attributed to Zr–Cl(T), Zr–Cl(B), Cl–Cl(B), and Cl-Cl(T), confirming its chain-like structure. Additionally, the peaks at \approx 4.01 and \approx 4.70 Å can be attributed to Zr–Zr and Zr-Cl atomic pairs between two neighboring [ZrCl_c] octahedra. For xLi₃PO₄@ZrCl₄ samples (Figure 2b), the peak intensity of both Zr-Cl(B) and Cl-Cl(B) pairs gradually decreases as x increases from 1/6 to 1/3; by contrast, the peak intensity of Zr—Cl(T) and Cl—Cl(T) remains unchanged. Therefore, it can be inferred that Li⁺ tends to coordinate with Cl(B), and the dissociation of Li₃PO₄ is closely related to the weakening of Zr-Cl(B) bonds. Moreover, the Zr–Zr pairs remain unchanged when x

16146840, 2025, 30, Downloaded from https://advanced.onlinelibrary.wiely.com/doi/10.1002/senm.202500913 by University Town Of Shenzhen, Wiley Online Library on [17/11/2025]. See the Terms and Condition (https://onlinelibrary.wiely.com/terms-

and-conditions) on Wiley Online Library for rules of use; OA articles are governed by the applicable Creative Commons

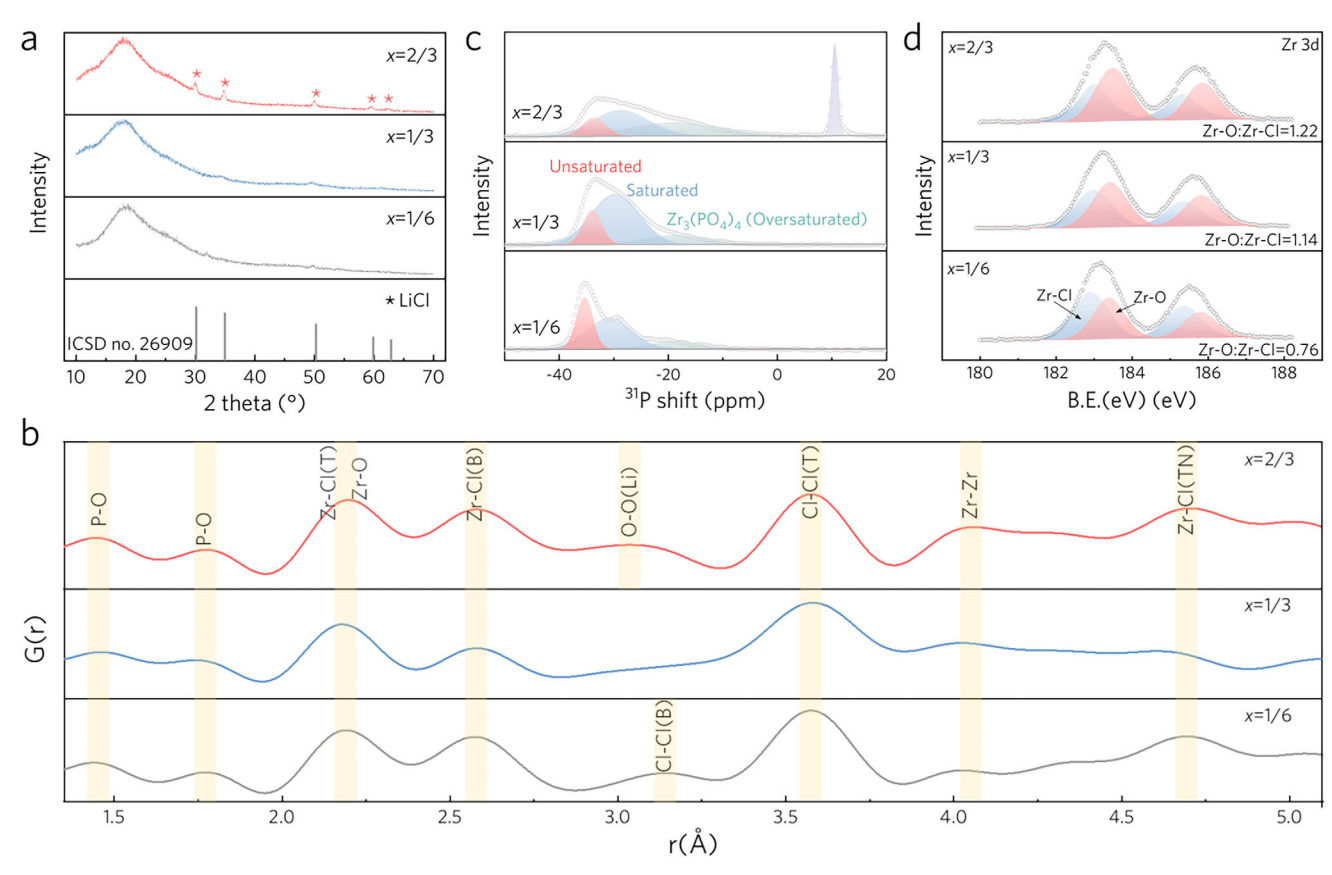


Figure 2. Characterization of $xLi_3PO_4@ZrCl_4$. a) XRD pattern of $xLi_3PO_4@ZrCl_4$ samples. b) PDF pattern of $xLi_3PO_4@ZrCl_4$ samples. c) NMR patterns of $xLi_3PO_4@ZrCl_4$ samples. d) XPS data of $xLi_3PO_4@ZrCl_4$ samples.

≤ 1/3, showing that the polymer-like ZrCl₄ structure is maintained before oversaturation. Since two adjacent Zr atoms connect via two Cl(B), it can be inferred that each Zr contributes one Cl(B) to coordinate with Li⁺, while the other Cl(B) maintains the chain structure. This explains why Li+ transport becomes saturated when the Li: Zr ratio reaches 1. The peaks at \approx 1.5 and \approx 1.8 Å, corresponding to the P—O atomic pair, indicate that the [PO₄] tetrahedra are well-preserved in the SSEs. To compensate for the weakened Zr-Cl(B) coordination, the unsaturated Zr bonds with O in the [PO₄] group (see Figure S16, Supporting Information). The newly formed Zr-O bond shares a similar peak position with Zr-Cl(T) at ≈2.19 Å. As the Li₃PO₄ content increases further (x = 2/3), the change in the peak shape of the Zr–Zr pair suggests partial disruption of the chain structure, which impedes Li⁺ transport and limits the salt dissociation by the matrix. Combined with the XRD results above, the precipitation of LiCl leads to the enhancement of the peak corresponding to its Cl-Cl bond (≈ 2.55 Å, similar to Zr–Cl(B)).[34] In addition, the peak for two O atomic pairs adjacent to the Li position (denoted as O—O(Li), \approx 3 Å) is observed. This is attributed to incompletely dissociated Li₃PO₄, which is undetected by XRD due to its minute quantity and low crystallinity. This phenomenon is analogous to ion aggregate-type solvated structures reported in liquid or polymer electrolytes.[35]

Solid-state nuclear magnetic resonance (ssNMR) was employed to further investigate the local structure changes $\frac{1}{2}$

(Figure 2c). Broad asymmetric signals centered \approx -33 ppm are observed in the ³¹P NMR spectra of xLi₃PO₄@ZrCl₄ SSEs, confirming the dominating amorphous phases. These asymmetric signals can be deconvoluted into three peaks at -35, -30, and -18 ppm, which indicate that PO₄ 3- dissociated in ZrCl₄ exists in at least three chemical environments, with no P-Cl bond formation.[36-38] As the concentration of Li₃PO₄ increases, the peak intensity at -35 ppm gradually decreases while the peak at -18 ppm corresponding to $Zr_3(PO_4)_4$ increases. [39,40] The downfield shift in the chemical shift could be attributed to the strong binding affinity between PO₄3- and Zr4+, which enhances the deshielding effect by reducing the electron cloud density around the phosphorus atom. The increase in the Zr₂(PO₄)₄ peak intensity indicates the continued dissociation of lithium salt, consistent with the XRD results. Therefore, these three chemical environments can be reasonably assigned to the unsaturated, saturated, and oversaturated (i.e., Zr₃(PO₄)₄ formation) states of PO₄³⁻ in the ZrCl₄ chain. Excessive Zr₃(PO₄)₄ configuration would disrupt the polymer-like chain and impair the dissociation ability of the matrix. Consequently, a new single peak of insufficiently dissociated Li₃PO₄ appears at 10 ppm in 2/3Li₃PO₄@ZrCl₄ (Figure S17, Supporting Information), in agreement with the PDF conclusions. Such a dissociation mechanism is further confirmed by the Fourier transform infrared (FTIR) results (Figure \$18, Supporting Information). The absorption peak of $v_3(PO_4^{3-})$ at 1014.3 cm⁻¹ blueshifted to high

16/14/840, 2025, 30, Downloaded from https://davanced.onlinelibrary.wiley.com/doi/10.1002/aemm.20250913 by University Town Of Shenzhen, Wiley Online Library on [17/11/2025]. See the Terms and Conditions (https://onlinelibrary.wiley.com/terms-and-conditions) on Wiley Online Library for rules of use; OA articles are governed by the applicable Creative Commons

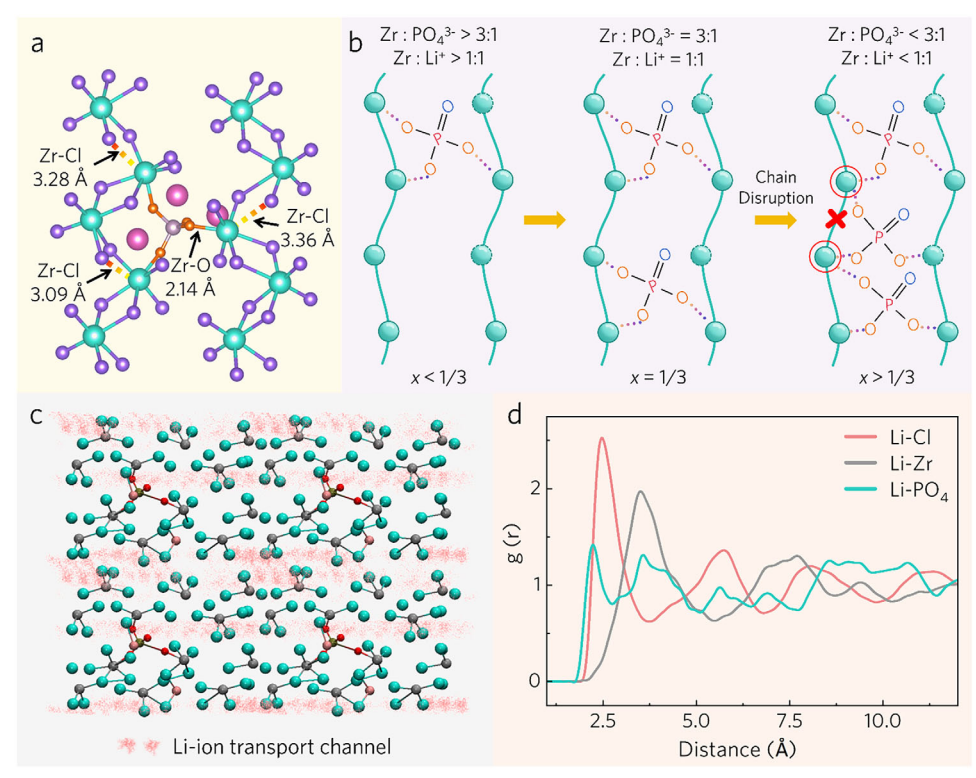


Figure 3. Salt dissociation mechanism and Li-ion transport channels. a) Geometry optimization of Li_3PO_4 and $ZrCl_4$. b) Scheme of the dissociation process of Li_3PO_4 in $ZrCl_4$. c) Proposed Li-ions transport pathway in $1/3Li_3PO_4@ZrCl_4$. d) The radial distribution function of the Li atom centered on the Cl, Zr, and PO_4 .

wavenumbers for $1/6\mathrm{Li_3PO_4} @\mathrm{ZrCl_4}$ and $1/3\mathrm{Li_3PO_4} @\mathrm{ZrCl_4}$, owing to the newly formed bonding between $\mathrm{PO_4}^{3-}$ and $\mathrm{Zr.}^{[41]}$ However, for $\mathrm{X}=2/3$, the undissociated $v_3(\mathrm{PO_4}^{3-})$ absorption peak was re-detected. The X-ray photoelectron spectroscopy (XPS) results further confirm the formation of Zr-O bonds (Figure 2d; Figure S19, Supporting Information). [42,43] As the amount of $\mathrm{Li_3PO_4}$ increases, the peak area ratio of Zr-O to Zr-Cl bonds rises from 0.76 to 1.22. This is attributed to the increased coordination of Zr-PO₄ $^{3-}$ and the breaking of Zr-Cl bonds, validating the dynamic dissociation process of lithium salts.

Similar to its Li-based counterparts, the XRD patterns (Figure S20, Supporting Information) indicate that xNa₃PO₄@ZrCl₄ samples exist in amorphous form, and NaCl impurity appears when the concentration of Na exceeds 1/3. The ³¹P NMR spectrum for the 1/3Na₃PO₄@ZrCl₄ samples is also dominated by broad, asymmetric signals, centered \approx –33 ppm (Figure S21, Supporting Information). Both XRD and NMR data suggest that xNa₃PO₄@ZrCl₄ possesses a very similar microstructure to xLi₃PO₄@ZrCl₄. With interchangeable anions and cations, our proposed SSE design strategy based on ZrCl₄ shows its versatility across a broad spectrum of battery systems.

2.3. Unveiling the Li-Ion Transport Mechanism

Based on the above results, the coordination of Li_3PO_4 in the ZrCl_4 matrix is illustrated in the geometry optimization (**Figure 3a**; Figure S22, Supporting Information), where $\text{PO}_4^{\ 3-}$ is

embedded between two parallel octahedral chains. One of the two Zr—Cl(B) bonds between two adjacent octahedrons breaks with the addition of Li $_3$ PO $_4$, forming a Zr—Cl—Li $^+$ and an unsaturated Zr. The unsaturated Zr will form Zr—O bonds with O in PO $_4$ 3 –, with a bond distance of 2.14 Å, which is consistent with the PDF data shown in Figure 2c. In this case, the chain structure of ZrCl $_4$ is maintained by the remaining Zr—Cl(B) bond. Since PO $_4$ is anchored to Zr, its mobility in SSE is compromised, which explains the high Li $^+$ transference number.

The critical influence of anion chemistry on salt dissociation is further highlighted through geometry optimization. Figure 3b illustrates the ideal process of Li₃PO₄ dissociation, where only three oxygen atoms in the PO₄³⁻ group participate in forming Zr—O bonds. When x is less than 1/3, sufficient Zr sites are available for complete salt dissociation, and the ZrCl₄ chains have not yet reached their maximum Li⁺ transport capacity. When x= 1/3, all Zr atoms will be coordinated with one PO_4^{3-} , hence the [ZrCl₆] octahedra are connected by exactly one Zr-Cl(B), and the ZrCl₄ chain is saturated with Li⁺ transport. As x exceeds 1/3, the chain structure can no longer accommodate excess Li₃PO₄ without breaking the remaining Zr–Cl(B) bonds, which results in the collapse of the ZrCl₄ chain structure as well as the precipitation of LiCl. These findings partially explain the three chemical environments of PO₄³⁻ observed in the ssNMR spectra, corresponding to the dynamic increase in Zr and PO₄³⁻ coordination. Similarly, the proposed model can also explain the ideal amount of other salts in ZrCl₄ (Figure S23, Supporting Information).

16146840, 2025, 30, Downloaded from https://advanced.onlinelibrary.wiley.com/doi/10.1002/aemm.20250913 by University Town Of Shenzhen, Wiley Online Library on [17/11/2025]. See the Terms and Conditions (https://onlinelibrary.wiley.com/terms-

and-conditions) on Wiley Online Library for rules of use; OA articles are governed by the applicable Creative Commons

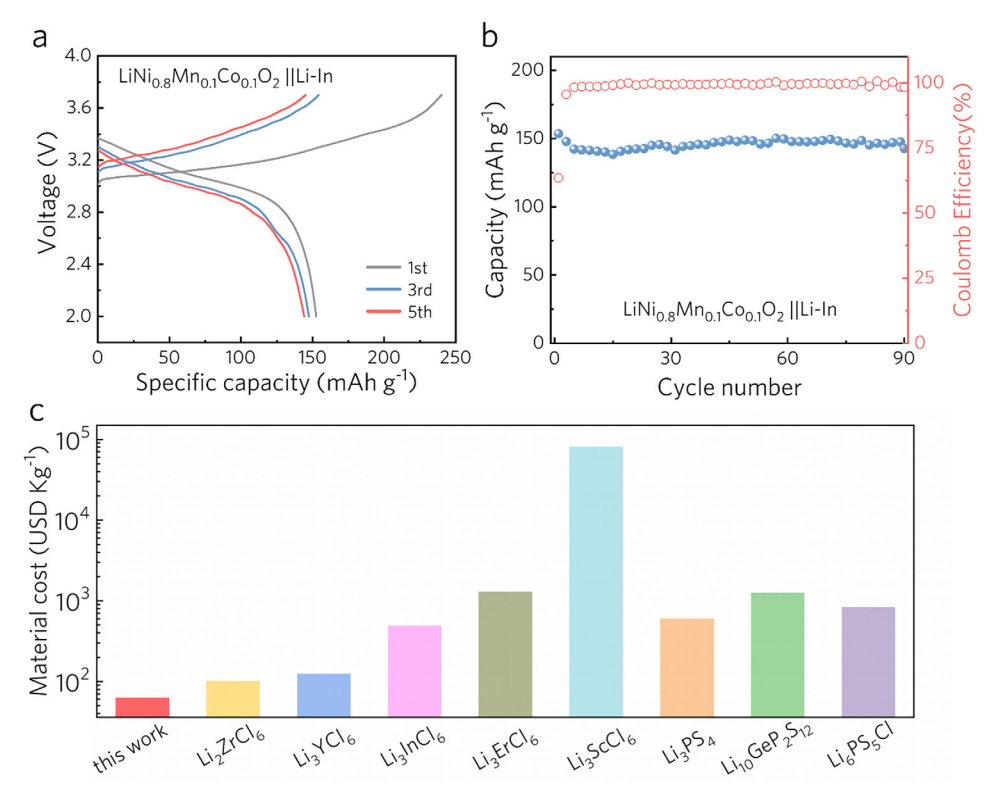


Figure 4. Cycling performance and costs of $1/3Li_3PO_4@ZrCl_4$. a,b) Charge–discharge curves and cycling performance of $1/3Li_3PO_4@ZrCl_4$ in a NMC811||Li-In cell at the current density of 0.1 mA cm⁻². c) Raw material costs for $1/3Li_3PO_4@ZrCl_4$ and reported SSEs based on bulk commodity prices (detailed information can be referred to Tables S3–S5, Supporting Information).

To further explore the Li-ion pathway in the as-prepared SSE, the dynamics of lithium migration are investigated by firstprinciples molecular dynamics methods based on a proposed local structure of 1/3Li₃PO₄@ZrCl₄ (Figure S24, Supporting Information). As visualized in Figure 3c, the free Li-ions from Li₃PO₄ have access to the ion tunnel formed by the arrangement of Cl atoms between neighboring ZrCl₄ chains. The viability of the favorable ion pathway is substantiated by the radial distribution function (RDF), where the highest peak for Li-Cl interactions at an average distance of 2.14 Å, signifying a strong bond between Li and Cl atoms (Figure 3d). Furthermore, the highest Li interaction energy with Cl, when compared to other atoms, provides additional support for the transport pathway facilitated by Cl (Figure S25, Supporting Information). Since the space between ZrCl₄ chains depends on the size of the anions embedded, the transport channel of Li⁺ can be modulated by anion groups. Compared with Cl⁻ and SO₄²⁻, PO₄³⁻ exhibits the largest size (Figure S26, Supporting Information) and the lowest anion number (due to the highest charge). With a broader pathway and more vacancies for Li⁺ transport, 1/3Li₃PO₄@ZrCl₄ is expected to show the highest ionic conductivity and the lowest activation energy.

2.4. Application Prospects in Full Cells

In addition to ionic conductivity, the interfacial stability of SSEs with cathode and anode materials, as well as their cost, determines their practical value. The electrochemical stability win-

dow of SEs is evaluated using linear sweep voltammetry with an asymmetric cell, where carbon black (CB)/SE composites serve as the working electrode and lithium metal act as the counter/reference electrode (Figure S27, Supporting Information). The introduced CB in the working electrode can provide sufficient electron transport, thus precisely monitoring the reaction potentials. $^{[44-46]}$ 1/3Li $_3$ PO $_4$ @ZrCl $_4$ exhibits a wide electrochemical stability window of 2.20–4.75 V versus Li $^+$ /Li. Similar to many chloride electrolytes, 1/3Li $_3$ PO $_4$ @ZrCl $_4$ displays a distinct cathodic current response above 0 V, suggesting that it is unstable toward Li metal. By contrast, 1/3Li $_3$ PO $_4$ @ZrCl $_4$ does not exhibit a significant anodic current even at ≈ 5 V, indicating strong oxidation resistance, making it suitable for high-voltage cathode materials.

To evaluate the application of $1/3\mathrm{Li}_3\mathrm{PO}_4 @ \mathrm{ZrCl}_4$ in high-voltage ASSLBs, full cells with $\mathrm{LiNi}_{0.8}\mathrm{Mn}_{0.1}\mathrm{Co}_{0.1}\mathrm{O}_2$ (NMC811) cathode and lithium-indium alloy (Li-In) anode were fabricated and tested. The NMC811||1/3Li_3\mathrm{PO}_4 @ \mathrm{ZrCl}_4||Li-In cell exhibits a reversible capacity over 153 mAh g $^{-1}$ (Figure 4a) between 2.0–3.8 V at 0.1 mA cm $^{-2}$ (25 °C, with NMC811 loading of 4.7 mg cm $^{-2}$). The ASSLB exhibited a reversible capacity of over 153 mAh g $^{-1}$. Stable cycling was achieved for 90 cycles, with a capacity retention of 92.9% (Figure 4b). Even at high current density (0.5 mA cm $^{-2}$) or high cathode mass loading (20.0 mg cm $^{-2}$), the $1/3\mathrm{Li}_3\mathrm{PO}_4$ @ ZrCl_4 -based ASSLB maintains stable cycling performance (Figures \$28–\$30, Supporting Information). Compared to the reported halide electrolytes, $1/3\mathrm{Li}_3\mathrm{PO}_4$ @ ZrCl_4 exhibits superior electrochemical performance and can withstand more

ADVANCED ENERGY MATERIALS

extreme full-cell testing conditions (Figures S31 and S32, Tables S1 and S2, Supporting Information). These results highlight the potential of $1/3 \text{Li}_3 \text{PO}_4 @ \text{ZrCl}_4$ with polymer-like ion transport behavior for future ASSLB applications.

Moreover, in view of the tight supply of global lithium resources and the sharp rise in lithium salt prices, lowering lithium content in SSEs without compromising Li⁺ conductivity is also desirable. Compared with other representative SSEs (Figure S33, Supporting Information), $1/3\text{Li}_3\text{PO}_4@Z\text{rCl}_4$ exhibits the lowest lithium content of 2.5 wt. More significantly, $1/3\text{Li}_3\text{PO}_4@Z\text{rCl}_4$ also exhibits obvious competitive advantages in cost over its counterparts (Figure 4c), which lends a substantial edge to its viability for commercial applications.

3. Conclusion

In summary, a new class of halide superionic conductors was synthesized by a mechanochemical method using inexpensive elements. In the 1D ZrCl4 matrix, Li/Na salts could be dissociated with a maximum Li (or Na): Zr ratio of 1:1. The released Li/Na ions can transport rapidly between octahedral ZrCl4 chains, resulting in high ionic conductivity. Simultaneously, the released anions are firmly anchored to ZrCl₄, yielding a Li-ion transference number close to 1. Moreover, the anion group embedded in the octahedra chain can modulate the transport channel of Li/Na ions, and then affect the ionic conductivity and activation energy. Among the as-prepared SSEs, 1/3Li₃PO₄@ZrCl₄ SSE exhibits the highest ionic conductivity at 1.2 mS cm⁻¹, low electronic conductivity, and wide electrochemical window, hence enabling long-term cycling of LiNi_{0.8}Mn_{0.1}Co_{0.1}O₂||Li-In cells. Demonstrating a new lithium-ion conduction mechanism and featuring interchangeable anions and cations, the proposed ZrCl₄-based electrolytes provide a versatile and innovative approach for designing advanced SSEs adaptable to diverse battery systems.

Supporting Information

Supporting Information is available from the Wiley Online Library or from the author.

Acknowledgements

Y.S., S.X., and Z.X. contributed equally to this work. This research was financially supported from the National Natural Science Foundation of China (No. 92472206, No.52102200), and the Shenzhen Science and Technology Planning Project (JSGG20220831095604008). The Major Science and Technology Infrastructure Project of Material Genome Big-science Facilities Platform supported by Municipal Development and Reform Commission of Shenzhen, International joint Research Center for Electric Vehicle Power Battery and Materials (No.2015B01015), Guangdong Key Laboratory of Design and calculation of New Energy Materials (No. 2017B030301013), Shenzhen Key Laboratory of New Energy Resources Genome Preparation and Testing (No. ZDSYS201707281026184).

Conflict of Interest

The authors declare no conflict of interest.

Data Availability Statement

The data that support the findings of this study are openly available in Supporting Information at https://doi.org/10.1002/aenm.202500913, reference number 5.

Keywords

chloride solid-state electrolyte, glass electrolyte, ion transport mode, solidstate battery

> Received: February 15, 2025 Revised: April 15, 2025 Published online: April 29, 2025

1614849, 2025, 30, Dwnholoded from https://atvanced.oninelibrary.wiely.com/oi/010.002/aem.20.250913 by University Town Of Shenzhen, Wiley Online Library on [17/11025]. Se the Terms and Conditions (https://onlinelibrary.wiely.com/terms-and-conditions) on Wiley Online Library for rules of use; OA articles are governed by the applicable Centwive Commons

- [1] A. Manthiram, X. Yu, S. Wang, Nat. Rev. Mater. 2017, 2, 16103.
- [2] J. Janek, W. G. Zeier, Nat. Energy 2023, 8, 230.
- [3] Q. Zhao, S. Stalin, C.-Z. Zhao, L. A. Archer, Nat. Rev. Mater. 2020, 5,
- [4] L.-Z. Fan, H. He, C.-W. Nan, Nat. Rev. Mater. 2021, 6, 1003.
- [5] K. Jun, Y. Chen, G. Wei, X. Yang, G. Ceder, Nat. Rev. Mater. 2024, 9, 887
- [6] Z. Li, J. Fu, X. Zhou, S. Gui, L. Wei, H. Yang, H. Li, X. Guo, Adv. Sci. 2023, 10, 2201718.
- [7] T. Famprikis, P. Canepa, J. A. Dawson, M. S. Islam, C. Masquelier, Nat. Mater. 2019, 18, 1278.
- [8] J. Ding, M. K. Gupta, C. Rosenbach, H.-M. Lin, N. C. Osti, D. L. Abernathy, W. G. Zeier, O. Delaire, Nat. Phys. 2025, 21, 118.
- [9] J. Mindemark, M. J. Lacey, T. Bowden, D. Brandell, *Prog. Polym. Sci.* 2018, 81, 114.
- [10] Y. Zheng, Y. Yao, J. Ou, M. Li, D. Luo, H. Dou, Z. Li, K. Amine, A. Yu, Z. Chen, Chem. Soc. Rev. 2020, 49, 8790.
- [11] S. C. Sand, J. L. M. Rupp, B. Yildiz, Chem. Soc. Rev. 2025, 54, 178.
- [12] Y. Fu, K. Yang, S. Xue, W. Li, S. Chen, Y. Song, Z. Song, W. Zhao, Y. Zhao, F. Pan, L. Yang, X. Sun, Adv. Funct. Mater. 2023, 33, 2210845.
- [13] L. Yang, Z. Wang, Y. Feng, R. Tan, Y. Zuo, R. Gao, Y. Zhao, L. Han, Z. Wang, F. Pan, Adv. Energy Mater. 2017, 7, 1701437.
- [14] X. Shan, Z. Song, H. Ding, L. Li, Y. Tian, A. P. Sokolov, M. Tian, K. Xu, P.-F. Cao, Energy Environ. Sci. 2024, 17, 8457.
- [15] S. Liu, L. Zhou, J. Han, K. Wen, S. Guan, C. Xue, Z. Zhang, B. Xu, Y. Lin, Y. Shen, L. Li, C.-W. Nan, Adv. Energy Mater. 2022, 12, 2200660.
- [16] Y. B. Song, K. H. Baeck, H. Kwak, H. Lim, Y. S. Jung, Adv. Energy Mater. 2023, 13, 2301142.
- [17] X.-X. Wang, D.-H. Guan, C.-L. Miao, J.-X. Li, J.-Y. Li, X.-Y. Yuan, X.-Y. Ma, J.-J. Xu, Adv. Energy Mater. 2024, 14, 2303829.
- [18] G. Jiang, C. Qu, F. Xu, E. Zhang, Q. Lu, X. Cai, S. Hausdorf, H. Wang, S. Kaskel, Adv. Funct. Mater. 2021, 31, 2104300.
- [19] F. Li, X. Cheng, G. Lu, Y.-C. Yin, Y.-C. Wu, R. Pan, J.-D. Luo, F. Huang, L.-Z. Feng, L.-L. Lu, T. Ma, L. Zheng, S. Jiao, R. Cao, Z.-P. Liu, H. Zhou, X. Tao, C. Shang, H.-B. Yao, J. Am. Chem. Soc. 2023, 145, 27774.
- [20] B. He, F. Zhang, Y. Xin, C. Xu, X. Hu, X. Wu, Y. Yang, H. Tian, Nat. Rev. Chem. 2023, 7, 826.
- [21] X. Li, J. Liang, X. Yang, K. R. Adair, C. Wang, F. Zhao, X. Sun, Energy Environ. Sci. 2020, 13, 1429.
- [22] D. Li, D. Yu, G. Zhang, A. Du, Z. Ye, Y. Jia, W. Hou, T. Xu, F. Li, S. Chi, Y. Zhu, C. Yang, Angew. Chem., Int. Ed. 2025, 64, 202419735.
- [23] H. Zhang, Z. Yu, J. Cheng, H. Chen, X. Huang, B. Tian, Chin. Chem. Lett. 2023, 34, 108228.
- [24] Y. Yu, Y. Huang, Z. Xu, Z. Wu, Z. Wang, G. Shao, Adv. Funct. Mater. 2024, 34, 2315512.
- [25] C. Wang, J. Liang, J. T. Kim, X. Sun, Sci. Adv. 2025, 8, adc9516.

ADVANCED ENERGY MATERIALS 16146840, 2025, 30, Downloaded from https://advanced.onlinelibrary.wiley.com/doi/10.1002/aenm.202500913 by University Town Of Shenzhen, Wiley Online Library on [17/11/2025]. See the Terms

and Conditions

for rules of use; OA

articles are governed by the applicable Creative Commons

www.advancedsciencenews.com

www.advenergymat.de

- [26] T. Dai, S. Wu, Y. Lu, Y. Yang, Y. Liu, C. Chang, X. Rong, R. Xiao, J. Zhao, Y. Liu, W. Wang, L. Chen, Y.-S. Hu, Nat. Energy 2023, 8, 1221.
- [27] G. M. Photiadis, G. N. Papatheodorou, J. Chem. Soc., Dalton Trans. 1998, 981.
- [28] H. Kwak, D. Han, J. Lyoo, J. Park, S. H. Jung, Y. Han, G. Kwon, H. Kim, S.-T. Hong, K.-W. Nam, Y. S. Jung, Adv. Energy Mater. 2021, 11, 2170045.
- [29] Y. Xu, L. Gao, L. Shen, Q. Liu, Y. Zhu, Q. Liu, L. Li, X. Kong, Y. Lu, H. B. Wu, Matter 2020, 3, 1685.
- [30] S. Xue, S. Chen, Y. Fu, H. Zhu, Y. Ji, Y. Song, F. Pan, L. Yang, Small 2023, 19, 2305326.
- [31] C. Wang, K. Fu, S. P. Kammampata, D. W. McOwen, A. J. Samson, L. Zhang, G. T. Hitz, A. M. Nolan, E. D. Wachsman, Y. Mo, V. Thangadurai, L. Hu, Chem. Rev. 2020, 120, 4257.
- [32] B. Shao, Y. Huang, F. Han, Adv. Energy Mater. 2023, 13, 2204098.
- [33] X. Shi, Z. Zeng, H. Zhang, Y. Huang, C.-H. Yan, Y. Du, Adv. Funct. Mater. 2023, 33, 2213638.
- [34] G. Wang, S. Zhang, H. Wu, M. Zheng, C. Zhao, J. Liang, L. Zhou, J. Yue, X. Zhu, Y. Xu, N. Zhang, T. Pang, J. Fu, W. Li, Y. Xia, W. Yin, X. Sun, X. Li, Adv. Mater. 2024, 37, 2410402.
- [35] J. Li, Z. Hu, S. Zhang, H. Zhang, S. Guo, G. Zhong, Y. Qiao, Z. Peng, Y. Li, S. Chen, G. Chen, A.-M. Cao, *Nat. Sustain.* 2024, 7, 1481.

- [36] B. Thomas, S. Paasch, S. Steuernagel, K. Eichele, Solid State Nucl. Magn. Reson. 2001, 20, 108.
- [37] A. S. Batsanov, S. M. Cornet, L. A. Crowe, K. B. Dillon, R. K. Harris, P. Hazendonk, M. D. Roden, Eur. J. Inorg. Chem. 2001, 2001, 1729.
- [38] D. Cheng, T. Wynn, B. Lu, M. Marple, B. Han, R. Shimizu, B. Sreenarayanan, J. Bickel, P. Hosemann, Y. Yang, H. Nguyen, W. Li, G. Zhu, M. Zhang, Y. S. Meng, Nat. Nanotechnol. 2023, 18, 1448.
- [39] M. Barre, M. P. Crosnier-Lopez, F. Le Berre, J. Emery, E. Suard, J.-L. Fourquet, Chem. Mater. 2005, 17, 6605.
- [40] M. Barré, F. Le Berre, M. P. Crosnier-Lopez, O. Bohnké, J. Emery, J. L. Fourquet, Chem. Mater. 2006, 18, 5486.
- [41] D. Liu, Z. Li, L. He, Z. Zhao, Desalination 2021, 514, 115186.
- [42] C. O. De González, E. A. García, Surf. Sci. 1988, 193, 305.
- [43] T. Tanabe, M. Tanaka, S. Imoto, Surf. Sci. 1987, 187, 499.
- [44] S. Deng, Y. Sun, X. Li, Z. Ren, J. Liang, K. Doyle-Davis, J. Liang, W. Li, M. Norouzi Banis, Q. Sun, R. Li, Y. Hu, H. Huang, L. Zhang, S. Lu, J. Luo, X. Sun, ACS Energy Lett. 2020, 5, 1243.
- [45] F. Walther, S. Randau, Y. Schneider, J. Sann, M. Rohnke, F. H. Richter, W. G. Zeier, J. Janek, *Chem. Mater.* **2020**, *32*, 6123.
- [46] X. Yang, Q. Yin, C. Wang, K. Doyle-Davis, X. Sun, X. Li, Prog. Mater. Sci. 2023, 140, 101193.
- [47] X. Sun, M. Ouyang, H. Hao, Joule 2022, 6, 1738.